Thermoelectric Power and Magnetic Permeability of $Cd_{0.4}Mn_{0.6}Co_xFe_{2-x}O_4$ ferrite system

T. M. Meaz*[*a], M. A. Amer,[a] M. A. Elkestawy[b], and A. I. Ghoneim[a].

[a]*Physics Department, Faculty of Science, Tanta University, Tanta, Egypt.*
[b]*Physics Department, Faculty of Science, Suez Canal University, Suez, Egypt.*

A series of Polycrystalline spinel ferrites with general formula $Cd_{0.4}Mn_{0.6}Co_xFe_{2-x}O_4$ (x=0.0, 0.125, 0.25, 0.375, 0.5, 0.75 and 1.00) were prepared by ceramic technique to study the effect of Co^{3+} ions substitution on their thermoelectric power, charge carrier concentration and charge carrier mobility at different temperatures. The compounds were characterized by X-ray, and IR spectra. X-ray diffraction pattern confirms the cubic single phase. Thermoelectric power values were found to be negative for all samples indicating that the majority of charge carriers are electrons. The relative magnetic permeability μ were measured as function of temperature. The phase transition temperatures were found to increase with increasing Co content.

1. Introduction:

During the last few years a lot of attention has been paid to the development of cobalt ferrite based materials due to its wide range of applications. Ferrites are iron containing complex oxides characterized by many interesting electrical and magnetic properties. They play a very useful role in many technological and magnetic applications because of their high electrical resistivity and sufficiently low dielectric losses over a wide range of frequencies [1, 2]. They are relatively inexpensive, stable, easily manufactured and widely used as both low- and high- frequency devices. Co-ferrite has very interesting properties where, the anisotropy of the Co ferrite can be used to compensate the negative anisotropies of other ferrites. The electrical and magnetic properties of many ferrites are found to change markedly by controlling the preparation conditions (the firing temperature and additives) [1, 3]. X-ray diffraction and IR spectroscopy are important tools to characterize ferrite samples [4-7]. Many authors had investigated several mixed ferrites such as; Cu–Co ferrites [8], Ca–Co ferrites [9], Co–Ge ferrites [10], $Co_{0.5}Zn_{0.5}Fe_2O_4$ [11], Ba–Co–Ti ferrites [12], Cd-Mn- ferrites [13], erbium substituted Mn–Zn ferrites [14], Mn–Zn–Gd ferrites [15], Cd-Cu- ferrites [16] and Ni–Cd ferrites

[17]. Up till now as far as the authors know there is no reports on investigation of the compositions $Cd_{0.4}Mn_{0.6}Co_xFe_{2-x}O_4$ (x=0.0, 0.125, 0.25, 0.375, 0.5, 0.75 and 1.00). Therefore, the aim of the present work is to investigate and report the thermoelectric power coefficient and the magnetic permeability of these compositions as function of temperature. In addition, from the thermoelectric power measurements it is intended to calculate both $\Delta\mu_d$ (the average change in charge carrier mobility) and Δn (the average change in charge carrier concentration) as functions of temperature to reveal the predominant type of conduction mechanism.

2. Experimental Technique:

2.1. Preparation of Samples

Ferrite samples having compositions $Cd_{0.4}Mn_{0.6}Co_xFe_{2-x}O_4$, x= 0.0, 0.125, 0.25, 0.375, 0.5, 0.75 and 1.00, were prepared using the standard ceramic technique [18]. X-ray diffraction analysis and IR spectroscopy were performed to ensure the formation of the required compositions [19]. The final fine powders were pressed into disc and toroid shaped samples at pressure 7×10^5 Torr and then sintered at 1473 ± 10 K for 24 hours. After being left to cool slowly to room temperature the samples were polished and their thickness were found to range from 0.2 to 0.4 cm. The disks were coated by a thin layer of silver paste that acts as a good contact for electrical measurements.

2.2. The thermo-electric power measurements:

The thermoelectric-voltage was measured by a digital multimeter of high precision. The sign of the thermo-voltage was determined from the polarity of the cold end of the sample since the charge carriers diffuse from the hot to the cold end. The thermoelectric power, α, was calculated using the relation [10]:

$$\alpha = \lim_{\Delta T \to 0} \frac{\Delta V}{\Delta T} \approx \frac{\Delta V}{\Delta T}$$

where ΔV is the measured potential difference across the sample and ΔT is the temperature difference between the two surfaces of the sample. The temperature gradient (ΔT/d) was kept nearly constant for all samples at all temperature values by adjusting the power of the sample heating coil for each particular thickness, d, to make the temperature gradient for all samples nearly around 10 K/cm.

Figure (1) shows the block diagram of the circuit used to measure the thermoelectric power coefficient α. The potential difference across the sample

is measured between the terminals 1 and 2 by a digital multimeter of the type 7562 YOKOGAWA. While the temperature of the two surfaces of the samples was measured by two thermocouples A and B.

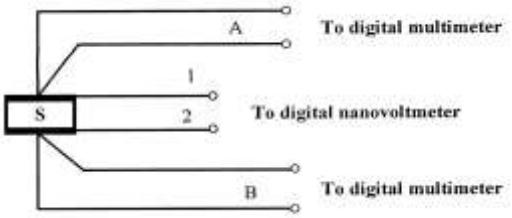

Fig. (1): Block diagram of the circuit used to measure thermoelectric power coefficient α, the terminals 1 and 2 are to measure the potential difference across the sample, the thermocouples A and B measure the temperature of the two surfaces of the sample S.

2.3. Permeability Measurements:

Figure (2) shows the resonance circuit used to determine the relative permeability μ for all compositions over a wide range of temperature [20].

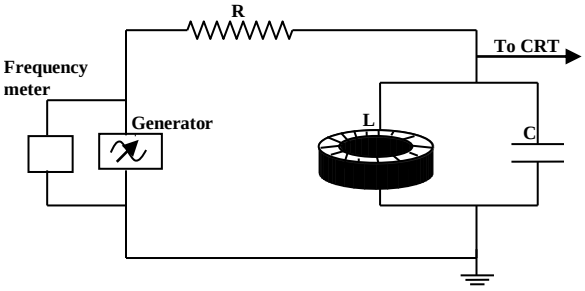

Fig.(2): A resonance circuit used to determine the permeability of a toroidal-shaped sample.

At resonance, if there is no stray capacitance: $1/\omega C = \omega L$; where $\omega = 2\pi f$, f is the frequency of the applied voltage at resonance, C is the value of the variable capacitance at resonance and L is the magnetic induction in the toroidal coil wound around the investigated ferrite core.
Therefore, the resonance frequency f is given by [21]:

$$f = \frac{1}{\left\{2\pi[L(C+C')]^{\frac{1}{2}}\right\}} \qquad (1)$$

;where C' is added to account for any stray capacitance involved in the circuit (such as at the input of the oscilloscope). From equation (1) we can see that

$$\frac{1}{f^2} = 4\pi^2 LC + 4\pi^2 LC' \qquad (2)$$

Plotting $\frac{1}{f^2}$ against C, we can determine L from the slope and consequently μ at each temperature value can be obtained, where the inductance L is related to the permeability μ by:

$$L = (N^2 A/D)\ \mu \times 10^{-8} \qquad \text{(Henry)} \qquad (3)\ [3]$$

where A is the cross section area of the toroidal-shaped core in cm^2, D is the average diameter in cm, and N is the number of winding of the coil.

3. Results and Discussion:

3.1. Thermoelectric Power Measurements:

Figure (3) illustrates the relation between the thermoelectric power **α** and $10^3/T$ for all studied samples in the temperature range from 318 K to 908 K. Thermoelectric power of all samples has a negative sign indicating that the majority charge carriers are electrons. The n-type charge carriers generally increases with increasing Co^{3+} ions content. Thermoelectric power **α** versus $10^3/T$ plot for each sample shows three distinct regions determined by two transition temperatures $T_{\alpha 1}$ and $T_{\alpha 2}$. From inspection of this figure, one can observe that below $T_{\alpha 1}$ the value of thermoelectric power, **α**, is approximately constant with temperature; above $T_{\alpha 2}$, **α** decreases in negativity with increasing temperature. Between $T_{\alpha 1}$ and $T_{\alpha 2}$ thermoelectric power increases in negativity with increasing temperature. From the anomalous behavior of , **α** ,with temperature may be illustrated as follows: at low temperatures the hopping mechanism by electrons is the predominant. As the temperature increases holes begin to contribute to the charge carriers transfer by hopping mechanism.

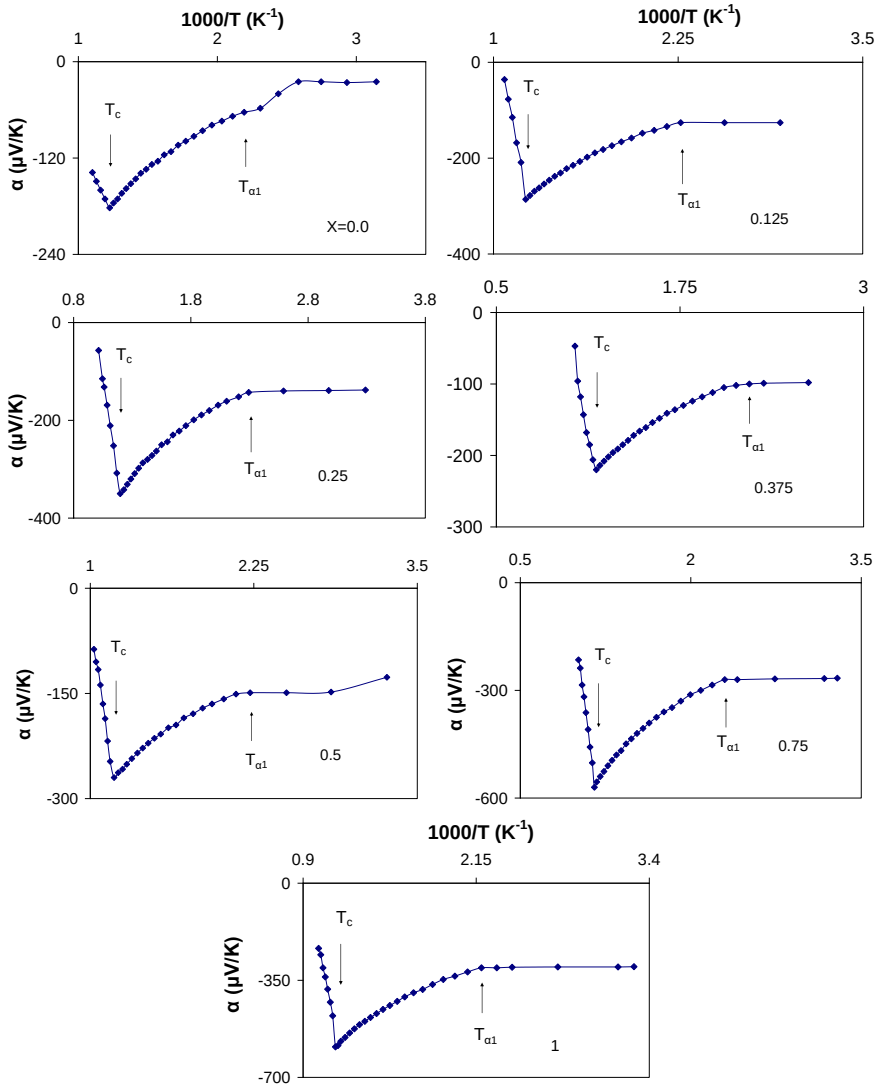

Fig (3): Thermoelectric power measurements for the investigated samples.

Table (1) shows that the values of transition temperatures from thermoelectric power measurements $T_{\alpha 1}$ and $T_{\alpha 2}$ for each sample. It is worth noting that these transition temperatures are in quite good agreement with the corresponding values in magnetic permeability measurements $T_{\mu 1}$, $T_{\mu 2}$.

Table (1): Effect of composition on the phase transition temperatures.

Composition	Thermoelectric power (α)		Initial magnetic permeability (μ)	
x	$T_{\alpha 1}$ (K)	$T_{\alpha 2}$ (T_c) (K)	$T_{\mu 1}$ (K)	$T_{\mu 2}$ (T_c) (K)
0.0	456	816	453	818
0.125	441	821	443	828
0.25	436	835	443	833
0.375	441	847	443	843
0.5	450	846	463	848
0.75	435	868	413	863
1	457	872	433	878

3.2. Charge Carrier Concentration (n):

The charge carrier concentration **n** is correlated to the thermoelectric power coefficient **α** by[22]:

$$n = (N_A/V)[1/(1+0.5Exp(-\alpha_e/k)] \qquad (4)$$

where V is the volume of the sample under study and N_A is the density of states. N_A is often taken as $10^{22}/cm^3$ in ferrites. Using equation (4), n values have been calculated for all samples at each temperature and ln n are plotted versus 1/T in Fig. (4).

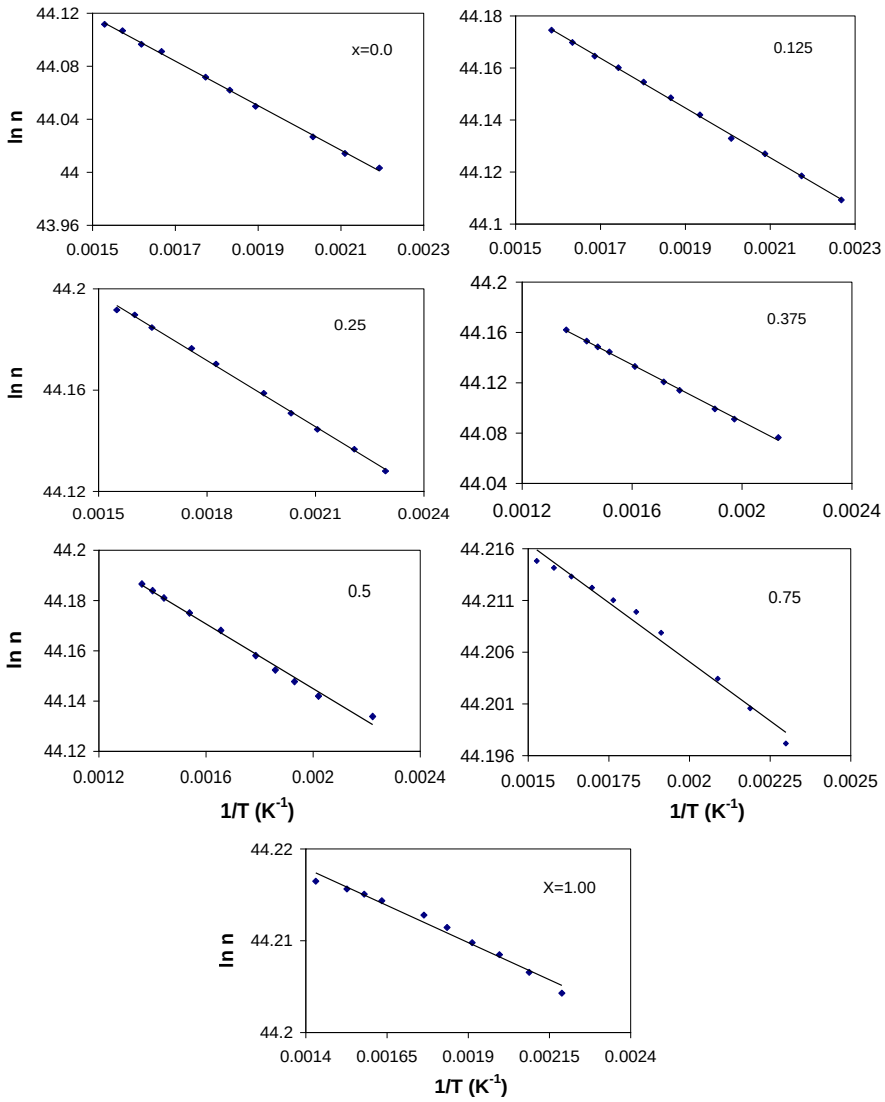

Fig. (4): Temperature dependence of the charge carrier concentration n for the investigated samples.

From inspection of Fig. (4) it is obviously seen that the charge carrier's concentration n is thermally activated since its values increase with increasing temperature. This may predict a suggestion that the band conduction mechanism contributes to the conduction process [19]. The activation energy of the generation charge carriers was determined from the slopes of the lines according to the following equation and is displayed as a function of composition in Table (2). $n_e = n_h = n_o Exp(-E_n/2kT)$ (5)

3.3. Charge carrier Mobility (μ_d) [23]**:**

The charge carrier's mobility $\boldsymbol{\mu_d}$ can be expressed by the following relation [3, 23]:

$$\sigma_{dc} = ne\mu_d$$

where σ_{dc} is the DC electrical conductivity of the sample. Using the calculated values of n from equation (4), the charge carriers mobility is calculated at each temperature for all samples and is represented as a function of temperature in figure (5) according to the following relation [23]:

$$\mu_d = (\mu_o/T)Exp[-E_H/KT]$$

From fig. (5) it is observed that ln $T\mu_d$ linearly increases with increasing temperature indicating that the charge carrier's mobility also is thermally activated which obviously reveals the contribution of the hopping mechanism to the conduction process [19]. The activation energy for the hopping process E_H was determined from the slopes of the lines according to the above equation and is given as a function of composition in Table (2). By comparing the values of the activation energy of the generation of charge carriers E_n and the activation energy of the charge carrier mobility E_h with those determined from the DC electrical conductivity measurements[19], we can see that E_n is much less than E_σ , whereas E_h is comparable to E_σ. This observation along with the experimental evidence that for a given temperature difference ΔT, the change in charge carrier mobility $\Delta\mu_d$ is larger than the change in charge carrier concentration Δn- which confirms that the predominant conduction mechanism is the hopping conduction rather than the band conduction. Similar results were observed [8, 9].

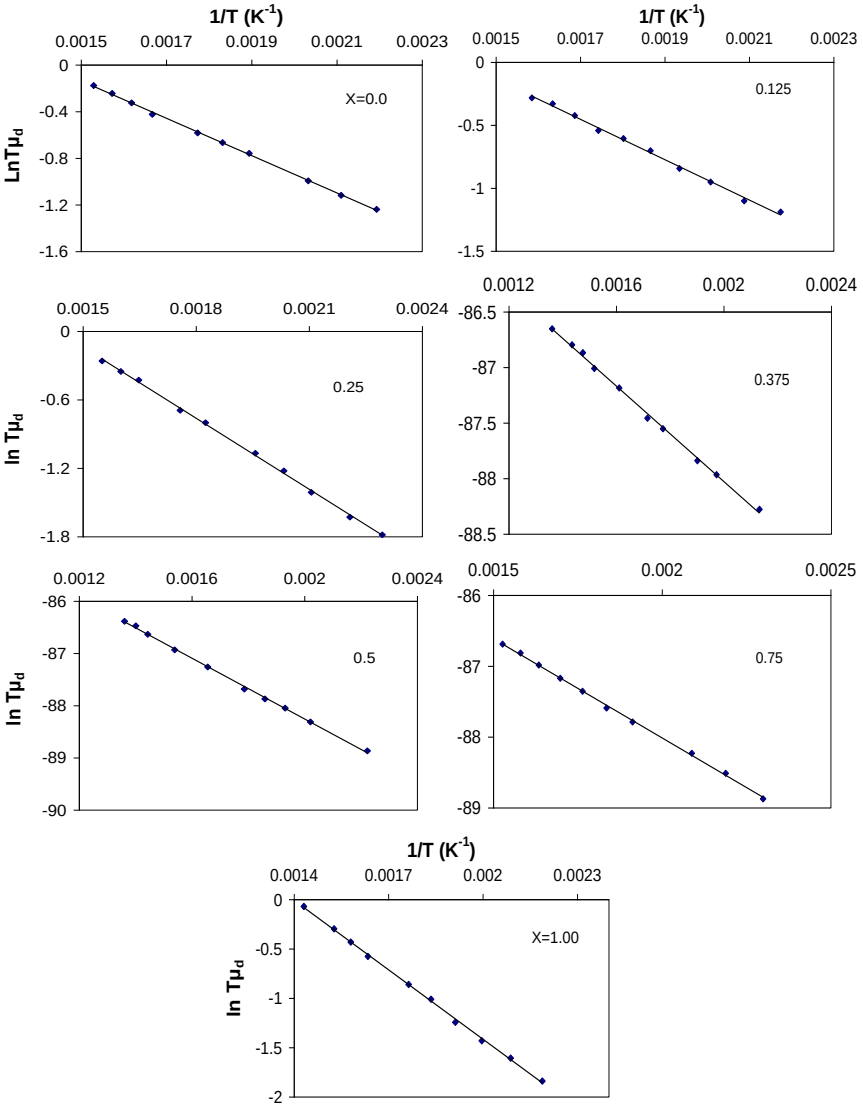

Fig. (5): Temperature dependence of the charge carrier mobility μ for the investigated samples.

Table (2): Composition dependence of the activation energies of generation of the charge carriers for the investigated samples.

x	E_σ (eV)	E_n (eV)	E_h (eV)
0.0	0.167	0.027	0.13964
0.125	0.155	0.013	0.14041
0.25	0.196	0.009	0.17854
0.375	0.205	0.019	0.18477
0.5	0.262	0.011	0.25034
0.75	0.245	0.099	0.14379
1	0.205	0.102	0.10216

3.4. Temperature dependence of the initial magnetic permeability

Figure (6) illustrates the temperature dependence of the relative permeability (μ) in the temperature range 914-293 K, for all the investigated samples. This figure shows that, μ increases slowly with increasing temperature up to a certain transition temperature T_i at which it decreases slowly and then increases slowly with increasing temperature up to a second transition temperature T_{ii} at which it drops rapidly [24-28]. The values of the transition temperature (T_{ii}) agree with the values of Curie temperature determined from thermoelectric power results within the experimental errors as shown in table (1). The first transition around 443 K may be due to changes in magneto-crystalline anisotropy constant. The second transition, at Curie temperature, is due to the magnetic-phase transition from ferrimagnetic to paramagnetic states [25].

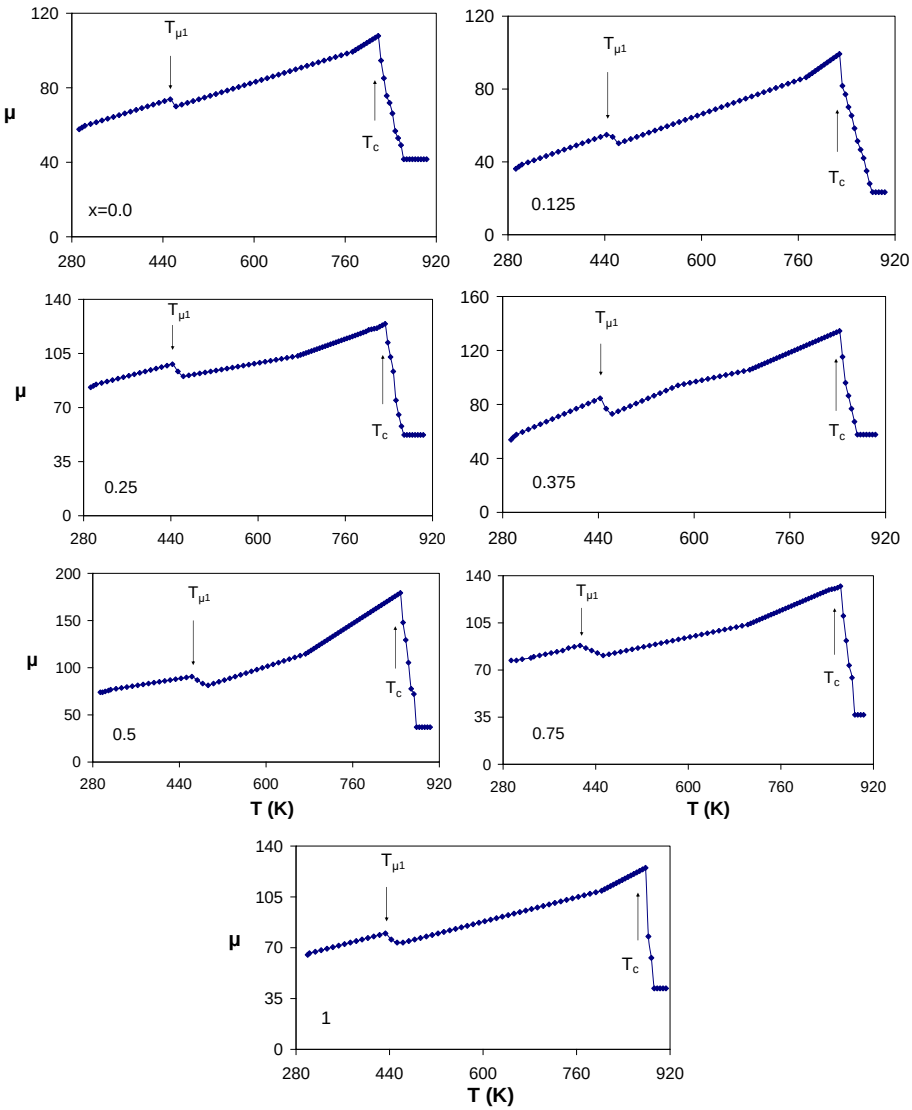

Fig. (6): Temperature-dependence of the relative permeability μ for the investigated samples.

Figure (7) also shows the relation between the Curie temperature T_c and the concentration of Co^{3+} content .From inspection of this figure it is reveals that the Curie temperature T_c is shifted to higher temperatures with increasing Co^{3+} ions substitution [29]. This behavior may be due to the replacement of Fe ions by the Co ions in octahedral sites [1].

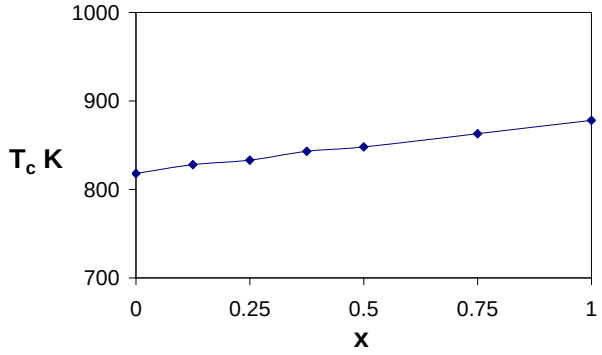

Fig. (7) : Composition dependence of Curie temperature.

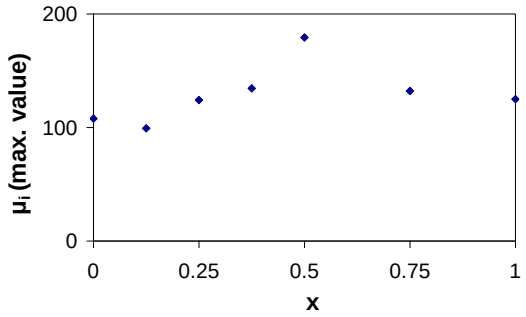

Fig. (8): Represents the variation of the maximum value of permeability as a function of composition. This behavior is the same as that found in IR, porosity, X-ray, crystal size and frequency exponent parameter for the same Ferrite samples [19].

4. Conclusion

From the above results, it can be concluded that:

(1) Thermoelectric power of all samples has a negative sign indicating that the majority charge carriers are electrons.

(2) The average change with temperature in charge carrier mobility $\Delta\mu_d$ is larger than the average change in charge carrier concentration Δn- confirming that the predominant conduction mechanism is the hopping conduction rather than the band conduction.

(3) The relative magnetic permeability μ increases slowly with increasing temperature up to a certain transition temperature T_i at which it decreases slowly and then increases again with increasing temperature up to a second transition temperature T_{ii} (Curie temperature) at which it drops rapidly. The Curie temperature is shifted to higher temperatures with increasing Co^{3+} ion substitution. (This behavior can

be explained due to the replacement of Fe ions by the Co ions in the octahedral sites.)

References

1. A. Goldman, "*Modern Ferrite Technology*", Van Nostrand Reinhold, New York, (1990).

2. W. D. Callister, Jr., "*Materials science and engineering an introduction*", 5th Edn., John Wiely & sons, Inc., USA, (1999).

3. J. Smit, H. P. Wijn, "*Ferrites*", John Wiley & sons, Inc., New York, (1959).

4. S. A. Patil, V. C. Mahajan, A. K. Ghatage, S. D. Lotke, *Mater. Chem. Phys*., **57**, 86 (1998).

5. P. N. Vasambekar, C. B. Kolekar, A. S. Vaingankar, *J. Magn. Magn. Mater*., **186**, 333 (1998).

6. A. M. M. Farea, S. Kumar, K. M. Batoo, A. Yousef, C. G. Lee, Alimuddin, *J. Alloy. Comp*., **464**, 361 (2008).

7. A. R. Shitre, V. B. Kawade, G. K. Bichile, K. M. Jadhav, *Mater. Letters*., **56**, 188 (2002).

8. Ch. Venkateshwarlu, D. Ravinder, *J. Alloys. Comp*., **426**, 4 (2006).

9. D. Ravinder, G. R. Kumar, Y. C. Venudhar, *J. Alloy. Comp*., **368**, 38 (2004).

10. D. Ravinder, A. C. S. Reddy, *J. Alloy. Comp*., **353**, 86 (2003).

11. A. S. Fawzi, A. D. Sheikh, V. L. Mathe, *J. Alloy. Comp*., **493**, 601 (2010).

12. D. Ravinder, P. Shalini, P. Mahesh, B. S. Boyanov, *J. Magn. Magn. Mater*., **268**, 154 (2004).

13. D. Ravinder, *Mater. Letters*, **44**, 130 (2000).

14. D. Ravinder, K.V. Kumar, *Mater. Letters*, **49**, 57 (2001).

15. B. R. Kumar, D. Ravinder, *Mater. Letters*, **53**, 441 (2002).

16. D. Ravinder, *Mater. Letters*, **43**, 129 (2000).

17. D. Ravinder, S. S. Rao, P. Shalini, *Mater. Letters*, **57**, 4040 (2003).

18. M. A. Amer, M. El Hiti, *J. Magn. Magn. Mater*., **234**, 118 (2001).

19. A. I. Ghoneim, " *M. Sc. Thessis, In Physics*", Tanta University, (2010).

20. S. A. Saafan, S. Magdiche, M. A. El-kestawy, A. Cheich-rouhou, *Physica Status Solidi* **(c)** 1, No. **7**, 1664 (2004).

21. S. A. Safaan, A. M. Abo El Ataa, M. S. El Messeery, *J. Magn. Magn. Mater*., **302**, 362 (2006).

22. S. A. Mazen, H. M. Zaki, *J. Magn. Magn. Mater*., **248**, 200 (2002).

23. C. Kittel, "*Introduction to Solid State Physics*", 5th Edn., Wiley Eastern Limited, New Delhy, (1977).

24. W. D. Kingery, H. K. Bowen, D. R. Uhlmann, "*Introduction to Ceramics*", 2nd Edn., Wiley-Inter science pub., (1975).
25. A. M. Abo El Ata, M. K. El Nimr, S. M. Attia, D. El Kony, A. H. Al Hammadi, *J. Magn. Magn. Mater*., **297**, 33 (2006).
26. M. A. Choudhary, J. Rahman, *J. Magn. Magn. Mater*., **223**, 21 (2001).
27. S. S. Bellad and B. K. Chougule, *Mater. Rev. Bulletin*, **8**, 1165 (1998).
28. R. G. Kharabe, S. A. Jadhav, A. M. Shaikh, D. R. Patil, B. K. Chougule, *Mater. Chem. Phys*., **72**, 77 (2001).
29. S. M. Yunus, H. Yamauchi, A. K. M. Zakaria, N. Igawa, A. Hoshikawa, Y. Haga, Y. Ishii, *J. Alloy. Comp*., **455**, 98 (2008).